Active Magnetostatic Wave Delay Line

Yuri K. Fetisov, *Senior Member, IEEE*, Pavel Kabos, *Senior Member, IEEE*, and Carl E. Patton, *Fellow, IEEE*

***Abstract*— Two configurations for an active microwave delay line with feedback to improve the loss per unit delay time have been made and characterized. The lines utilized thin yttrium iron garnet (YIG) film, magnetostatic wave (MSW) passive elements, a microwave amplifier, and a variable attenuator connected in a feedback loop. The two delay line setups used a surface wave (MSSW) configuration with a single YIG element and a nondispersive configuration with MSSW and backward volume wave (MSBVW) delay lines in series. For each setup, a sequence of delayed pulses at the output is observed when a single microwave pulse is fed to the input. The one-pass delay time T of the pulse through the MSW delay line and the number n of circulations in the feedback loop defines the total delay time nT for the nth pulse. The feedback resulted in a reduction in the output pulse decay rate and longer useful delay times. For a passive delay line with no feedback, typical values of the loss p.u. delay time L and useful delay time $(nT)_U$ were -110 dB/μs and 0.1–0.2 μs, respectively. With feedback for the MSSW delay line, a 4.5-GHz operating frequency, and 40 ns input pulses, L and $(nT)_U$ were -19 dB/μs and 0.6 μs, respectively. Feedback with the nondispersive delay line gave L and $(nT)_U$ values of -12 dB/μs and 3 μs, respectively, for 4.5-GHz, 40-ns input pulses.**

***Index Terms*—Active delay line, dispersive delay line, electronically controlled delay line, magnetostatic backward volume wave, magnetostatic surface wave, magnetostatic wave, microwave delay line, microwave feedback, nondispersive delay line, passive delay line, variable delay line, yttrium iron garnet.**

NOMENCLATURE

MSW	Magnetostatic wave.
YIG	Yttrium iron garnet.
f_o	Operating point carrier frequency.
T	MSW delay line one pass delay time.
I	MSW delay line one pass insertion loss.
H_{ext}	Static external magnetic field.
Λ	Length of the MSW propagation path.
V_g	MSW group velocity.
L_P	Propagation losses per unit time.
ΔH	Uniform mode ferromagnetic resonance half-power line width.
C	Loss coefficient on the order of unity defined by L_P [dB/μs] $\simeq -76C\Delta H$ [Oe].
FMR	Ferromagnetic resonance.
MSSW	Magnetostatic surface wave.
MSBVW	Magnetostatic backward volume wave.
A	Attenuation of feedback loop variable attenuator.
G	Gain of microwave amplifier in feedback loop.
B_{in}	Coupling coefficient of input directional coupler.
B_{out}	Coupling coefficient of output directional coupler.
GGG	Gallium gadolinium garnet.
MSFVW	Magnetostatic forward volume wave.
T_o	Input microwave pulsewidth.
P_{in}	Input microwave pulse peak power.
P_{out}	Output microwave pulse peak power.
n	Number of passes through the YIG film delay line.
$P_{\text{out}}(n)$	Output microwave pulse peak power after n passes.
nT	Total delay time after n passes.
Γ	Total gain in the feedback loop without interference effects.
f_k	General magnetostatic wave frequency.
k	General magnetostatic wavenumber.
$F(k)$	Dispersion relation function defined by $f_k = F(k)$.
k_o	Operating point carrier wavenumber.
λ_o	Operating point carrier wavelength.
S	YIG film thickness.
NLS	Nonlinear Schrödinger equation.
z	Propagation direction.
t	Time.
$u(z,t)$	Complex scalar envelope function which represents the MSW wave packet dynamic magnetization amplitude.
$\mathbf{m}$	Dynamic magnetization response for the MSW signal.
M_s	Saturation magnetization of the YIG material.
η	Temporal MSW relaxation rate.
γ	Electron gyromagnetic ratio.
D	Dispersion coefficient defined according to $D = 2\pi\partial^2 F(k)/\partial k^2\|_o$ and evaluated at the operating point $(f_o,\ k_o)$.
N	Nonlinear coefficient defined by $N = 2\pi\partial E(k,\|u\|^2)/\partial\|u\|^2\|_o$ and evaluated in the $u \to 0$ limit and at the $(f_o,\ k_o)$ operating point.
f_H	Internal static field in frequency units parameter defined according to $f_H = (\|\gamma\|/2\pi)H$.
f_M	Magnetization in frequency units parameter defined according to $f_M = (\|\gamma\|/2\pi)\cdot 4\pi M_s$.
H	Static internal magnetic field.
f_B	MSSW lower band edge frequency and MSBVW upper band edge frequency in the $k = 0$ limit,

Manuscript received March 11, 1997; revised July 1, 1997. This work was supported in part by National Science Foundation under Grant DMR-9400276 and by the U.S. Army Research Office under Grant DAAH04-95-1-0325.

Y. K. Fetisov is with the Department of Physics, Colorado State University, Fort Collins, CO 80523 USA, on leave from the Moscow Institute of Radio Engineering, Electronics, and Automation (MIREA), Moscow, Russia (e-mail: fetisov@orc.ru).

P. Kabos is with the Department of Physics, Colorado State University, Fort Collins, CO 80523 USA, on leave from the Slovak Institute of Technology, Bratislava, Slovakia (e-mail: kabos@lamar.colostate.edu).

C. E. Patton is with the Department of Physics, Colorado State University, Fort Collins, CO 80523 USA (e-mail: patton@lamar.colostate.edu).

Publisher Item Identifier S 0018-9464(98)00113-7.

given by $f_B = [f_H(f_H + f_M)]^{1/2}$.

L Total loss per unit delay time.

$(nT)_U$ Cumulative useful delay time.

$u_o(t)$ Gaussian scalar envelope function for the time dependent input pulse launched at $z = 0$ with a peak at $t = 0$.

μ_o Peak amplitude of $u_o(t)$ Gaussian input pulse.

Δ_o Width parameter for $u_o(t)$ Gaussian input pulse.

Z Position of detection of Gaussian pulse relative to position of peak at launch at $t = 0$ and to $z = 0$.

τ Time of detection of the peak of the Gaussian input pulse $u_o(t)$ at $z = Z$.

T_d Dispersion time.

$u_\tau(t)$ Complex time profile for propagated Gaussian pulse at $z = Z$ with a peak at $t = \tau$.

Δ_τ Width parameter for $u_\tau(t)$ pulse.

μ_τ Peak amplitude of $u_\tau(t)$ pulse.

$W(f)$ Fourier frequency distribution $W(f)$ for a square pulse of amplitude μ_o, width T_o, and with carrier frequency f_o.

I. Introduction

MAGNETOSTATIC wave (MSW) signals in thin YIG films have properties that are useful for the design of planar ferrite microwave-signal processing devices. In the 1–20 GHz microwave-frequency regime, for example, the group velocity and wavelength of MSW signals are smaller than the velocity and wavelength of electromagnetic waves in coaxial cable or dielectric waveguides by several orders of magnitude. For this reason, MSW excitations in strip line device structures are very promising for the design of miniature microwave delay lines. During recent years, many detailed investigations of MSW characteristics in strip line device structures have been carried out [1], [2]. Different types of MSW delay lines have been designed. These include dispersive delay lines [3], nondispersive delay lines [4], and electronically controlled delay lines with a variable delay time [5].

The most important characteristics of such MSW delay lines are the operating point carrier frequency f_o, the one-pass delay time T, and the insertion loss I. Choices for f_o depend on the ferrite structure parameters, the design of the line, and the magnitude and direction of static-external magnetic field H_{ext}. A change of H_{ext} from 0.1 to 10 kOe, for example, allows f_o to be changed from several hundreds of megahertz to 30 GHz or so. The delay time is determined by the length of the propagation path Λ and the magnitude of the MSW group velocity V_g. For a typical Λ-value of 1 cm or so and $|V_g|$ in the 10^6–10^8-cm/s range, delay times in the 10 ns–1 μs range are possible.

The total insertion loss of MSW delay lines comprises three main contributions: The microwave input to MSW conversion losses, the MSW propagation losses in the ferrite film, and the MSW to microwave output conversion losses. Methods developed for MSW excitation and detection with narrow strip line transducers [6] allow the conversion losses to be as low as -1–-10 dB, depending on the frequency band and the MSW configuration.

The propagation losses are related to the ferrite film and substrate properties as well as to the MSW loss and propagation characteristics. These losses are controlled mainly by the magnetic damping in the film. Expressed in terms of loss per unit (p.u.) delay time, these losses may be approximated as L_P [dB/μs] $\simeq -76\ C\Delta H$ [Oe]. The ΔH parameter is the uniform-mode FMR half-power line width. The C parameter is a coefficient on the order of unity that depends on the frequency band and the MSW configuration [7]. It follows that MSW delay lines based on YIG films with narrow FMR line widths in the 0.5–1-Oe range will have a total insertion loss of -50 to -100 dB/μs. In practice, it is the level of insertion loss that limits the maximum useful delay time. Typically, the maximum useful delay time for MSW delay lines is in the 100–300-ns range.

The above limitations are severe. Microwave delay lines with delay times of 1–10 μs or more, at reasonable levels of insertion loss, are required for many applications. Such requirements provide a strong motivation for further investigation of the loss characteristics of MSW delay lines as well as development of new methods to decrease or compensate for such losses. Several approaches are possible. One solution would be simply to connect a microwave amplifier to the delay line output. One could then obtain, in principle, a small net loss and large delay times by combining two or more MSW delay line-amplifier units in series [8]. This approach, however, introduces numerous complications into the design of the overall device and does not represent an optimum solution.

A more promising approach is to produce an active MSW delay line containing a passive MSW delay line and a microwave amplifier connected in a feedback loop. In such a scheme, a microwave pulse applied to the line input creates a sequence of microwave pulses at the line output with a pulse-to-pulse separation equal to the one-pass delay time T for the passive device alone. One can obtain reduced decay for the overall output pulse train and large overall delay times by adjusting the gain in the feedback to a value that is close to unity but still below the threshold for self-oscillation.

Similar recirculating delay line schemes have been used in optical communication systems [9]. These lines use a single-mode nondispersive low-loss optical fiber to delay the pulses and an Er-doped optical fiber amplifier to compensate for propagation losses. A maximum delay time of about 30 μs for optical pulses of 1 ns duration has been obtained in linear operation [10]. Delay times up to 100 μs have been obtained for optical solitons [11].

Until now, however, the application of this approach to microwave MSW delay lines has been limited. Microwave feedback schemes have been investigated only for those cases in which the total small signal loop gain exceeded unity and stable self-oscillations took place. Low noise electrically-tuned microwave oscillators for the 1–20-GHz frequency range have been designed on this basis [12], [13]. To the authors' knowledge, the use of feedback to produce an active MSW delay line has not been investigated, either theoretically or experimentally. The objective of this paper was to undertake

such an investigation. This paper describes the principle of operation, the design, experimental results, and various theoretical implications for an active microwave delay line with a passive MSW delay line and a microwave amplifier connected in a feedback loop.

Section II gives an overview of the active MSW line arrangement, gives design considerations for the passive MSW delay line element, explains the principle of formation for the microwave pulse train at the active line output, and describes the experimental setup for the measurements.

Section III presents results on the magnetostatic surface wave (MSSW) configuration. In Section III-A, results are presented on the loss and delay characteristics for a passive MSSW delay line. In Section III-B, these results are extended to an active delay line configuration with the passive MSSW delay line in the feedback loop. The influence of the total loss in the loop, the dispersion of the MSSW signal, the MSSW line-frequency response, and input microwave pulsewidth on the active line characteristics are considered.

Section IV presents additional results for an active delay line with a nondispersive MSW delay line in the feedback loop. In order to eliminate dispersion effects, a two-stage passive delay line was used. This line consisted of one magnetostatic backward volume wave (MSBVW) line and one MSSW line connected in series.

Overall, the results indicate that feedback may be used to achieve a reduced loss per unit (p.u.) delay-time performance factor and longer useful delay times.

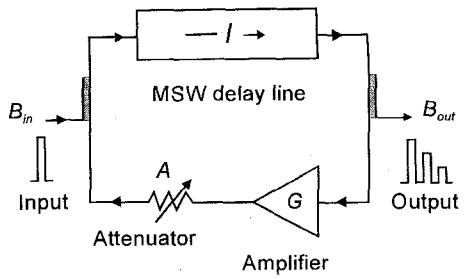

Fig. 1. Schematic diagram of the active MSW delay line with an attenuator, an amplifier, and a passive MSW-YIG film delay line in a feedback loop, and with directional couplers for input and output. The parameters I, A, G, $B_{\rm in}$, and $B_{\rm out}$ denote the gain or attenuation factors, or coupling coefficients, for the indicated elements.

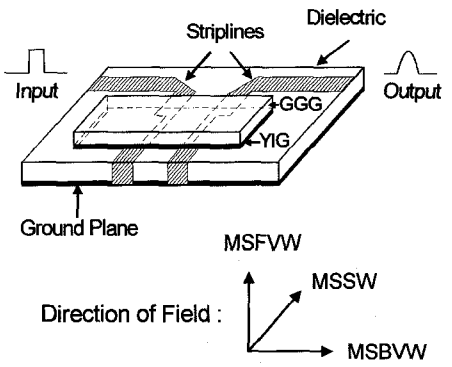

Fig. 2. Schematic diagram of the passive MSW delay line, with a YIG film on a GGG substrate, input and output transducers on a dielectric substrate with a bottom ground plane, and input and output microwave pulse signals as indicated. The three directions of the external static magnetic field shown in the bottom diagram correspond to the three basic kinds of excitations, MSSW, MSBVW, and MSFVW.

II. Active MSW Delay Line Design, Principle of Operation, and Measurement Details

A. Design Considerations

The design of the active MSW delay line is shown schematically in Fig. 1. The device contains a variable attenuator of attenuation A, a microwave amplifier of gain G, and a passive MSW YIG delay line with insertion loss I connected in a feedback loop. Two microwave directional couplers (DC's) with coupling coefficients $B_{\rm in}$ and $B_{\rm out}$ are used to couple microwave pulses in and out of the device. Note that the loop circulation is counterclockwise and the propagation of the MSW pulse through the passive delay line element is from right to left. The diagram shows one input pulse and a sequence of output pulses to indicate schematically the regenerative nature of the circuit. The delay time between individual output pulses is controlled by the passive MSW delay line characteristics. The decay or loss in output-pulse amplitude is controlled by the insertion loss of the passive delay line and the net gain in the feedback loop.

A single passive MSW-YIG film delay line element is shown in more detail in Fig. 2. This delay line contains a long and narrow YIG film strip on a gadolinium gallium garnet (GGG) substrate. Two strip line transducers on an alumina substrate are used to convert the input microwave signal into a propagating MSW signal in the YIG film and then to detect the MSW signal at the output. The YIG film is placed in close contact with the transducers. The entire delay line structure is placed in a uniform static-external magnetic field $H_{\rm ext}$. The vector diagram below the delay line diagram indicates the three basic MSW configurations for the device. Propagating MSSW signals and MSBVW signals result for in-plane fields when the field direction is perpendicular and parallel to the propagation direction, respectively [14]. Propagating MSFVW signals result when the static field is perpendicular to the YIG film [15]. The useful frequency band for the MSW signals depends on the magnitude of the field and the configuration. The MSSW and MSBVW configurations will be used for the devices described below. For the device presented in Section III, a single MSSW element was used. For the Section IV configuration, an MSSW and an MSBVW device were used in series to produce a passive line with a nondispersive delay characteristic. The relevant properties of MSSW and MSBVW excitations will be introduced as needed in these sections.

As indicated above, there are three important parameters for the passive delay line: the operating-point carrier frequency f_o, the one-pass delay time T, and the insertion loss I. For the analysis here, it is assumed that the input microwave pulsewidth T_o is much larger than the period of the microwave oscillation $1/f_o$, where f_o is in hertz. It is also assumed that f_o is within the MSW passband and no closer than $1/T_o$ or so to either band edge. Under these conditions, T is given by $T(f_o) = \Lambda/V_g(f_o)$, where Λ is the transducer separation and

$V_g(f_o)$ is the MSW pulse group velocity. The insertion loss, taken as $I(f_o)$, is also frequency-dependent. This is because longer delay times lead to more decay. These parameters will be considered in more detail below.

B. Principle of Operation

Turn now to the feedback and coupling elements shown in Fig. 1 and the basic operation of the active delay line. For this analysis, it is assumed that the feedback amplifier is wideband and has a frequency-independent gain coefficient G within the MSW passband. The attenuation A and the coupling coefficients $B_{\rm in}$ and $B_{\rm out}$ will also be taken to be independent of frequency. All gain or loss factors will be specified in dB, unless otherwise indicated, such that a negative value denotes a gain factor less than unity and a positive value denotes a gain factor greater than unity.

The microwave pulse with carrier frequency f_o, pulse duration T_o, and peak power $P_{\rm in}$ is applied to the input DC. For clockwise circulation as shown in Fig. 1, this input signal is first applied to the passive delay line. This pulse is picked up by the MSW-YIG film delay line input transducer and excites an MSW packet that propagates in the YIG filmstrip. The output transducer then picks up the MSW signal and converts it back to a microwave pulse. This first pass-delayed pulse is then coupled to the output port with an output pulse amplitude $P_{\rm out}$. This signal is also routed around the feedback loop amplifier and attenuator and back to the delay line. As the circulation continues, additional output pulses are produced. Note that both the pulse shape and pulsewidth may be modified from the input pulse due to the characteristics of the passive MSW delay line, the power level, etc. For this discussion, it is assumed that the input pulsewidth T_o is less than the one-pass delay time T. The electronic delay times, due to the cables, amplifier, etc., are relatively short compared to the delay from the YIG film device and these times are not included here.

It will be important to keep track of the output pulse delay and power as a function of the number of passes through the YIG film delay line. Let this number of passes be denoted as n. The peak power of the output pulse after n passes will be denoted as $P_{\rm out}(n)$. For n passes through the passive delay line, there will also be a cumulative pulse delay of nT. The power versus time diagram in Fig. 3 shows the basic output pulse sequence relative to the input pulse. In order to keep the diagram simple, the pulsewidth and pulse shape are taken to remain unchanged throughout the sequence. The first output pulse that experiences no delay due to the YIG film device is indicated with dashed lines and starts at time zero. The delayed sequence of output pulses occur at $T, 2T, \cdots, nT, (n+1)T$, etc., and with amplitudes $P_{\rm out}(n)$.

Simple considerations of the gain and attenuation factors for the circuit in Fig. 1 can be used to obtain the peak power for a given output pulse which is formed after n passes through the passive delay line and is delayed from the input pulse reference by a delay time of nT

$$P_{\rm out}(n) = P_{\rm in}B_{\rm in}AGB_{\rm out}[(1-B_{\rm in})(1-B_{\rm out})AGI(f_o)]^{n-1}. \quad (1)$$

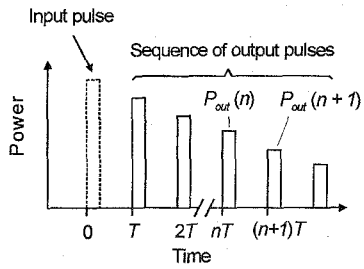

Fig. 3. Simplified illustration of a sequence of microwave pulses generated from the active MSW delay line by an input microwave pulse. The time T is the one-pass delay time, n is the number of passes through the feedback loop, and $P_{\rm out}(n)$ denotes the output peak power for the nth pulse.

The I, G, A, $B_{\rm in}$, and $B_{\rm out}$ parameters were defined above. When written in product form as in (1), the I, A, $B_{\rm in}$, and $B_{\rm out}$ attenuation parameters will be numbers between zero and one and the amplifier gain parameter G can range from zero upward. The ratio of peak powers for two pulses in sequence after $(n+1)$ and n passes is the same as the gain for the complete feedback loop

$$\frac{P_{\rm out}(n+1)}{P_{\rm out}(n)} = \Gamma(f_o) = (1-B_{\rm in})(1-B_{\rm out})AGI(f_o). \quad (2)$$

It follows from (2) that one can reduce the pulse-to-pulse decay of the sequence of delayed pulses and realize a large usable delay time by adjusting the total gain Γ in the feedback loop to a value that is close to unity but below the threshold for self-oscillation. One may achieve this condition with an amplifier of sufficient gain G and an appropriate adjustment of the attenuation A. A microwave pulse with the desired delay time may then be extracted from the output pulse sequence through the use of a clock-synchronized microwave switch.

There are several peculiarities of MSW delay lines and microwave amplifiers that can significantly affect the response characteristics of the passive and active devices described above. The discussion below will introduce the basic effects and parameters that are needed to describe these influences. Specifics for the MSSW and MSBVW configurations will be introduced as needed in the sections which follow.

First, there are the purely linear effects at very low-power levels. The linear delay-line response comes mainly from the lowest order MSW dispersion branch for the configuration of interest. This dispersion branch is characterized by a frequency f_k versus wavenumber k dispersion relation defined by $f_k = F(k)$, where $F(k)$ is a particular function for the configuration of interest. A chosen f_o within the MSW passband selects out a particular operating point at $f_k = f_o$ and $k = k_o$. Any variation in f_o results, therefore, in a change in the MSW carrier wavenumber k_o, the wavelength $\lambda_o = 2\pi/k_o$, and the pulse signal group velocity $V_g(f_o) = 2\pi\partial F(k)/\partial k|_o$. The subscript "$o$" indicates that the derivative is evaluated at $k = k_o$.

There are two basic low-power effects. First, the change in the MSW carrier wavelength λ_o with frequency results in a variation in the strip-line transducer conversion efficiency between the input and output microwave signal and the MSW excitation. Second, the frequency-dependence of V_g results in a variation of the MSW propagation loss. A lower V_g

means a longer propagation time and, hence, more decay due to relaxation. As a result of all these variations, the overall insertion loss I of the MSW delay line will depend on frequency. This is the motivation for the use of $I(f_o)$ in (1) and (2). Typically, the frequency response of the MSW delay line will have one maximum within the passband.

There are additional considerations when narrow pulses are propagated. For narrower pulses, more Fourier frequency components are needed to construct the pulse. These different frequency components travel at different phase velocities and lead to dispersion-broadening. The same frequency-broadening for narrow pulses gives rise to additional distortion because of the frequency-dependent coupling and loss considerations noted above. Narrow pulses also present the possibility of cutoff effects. If the frequency spectrum of the microwave pulse extends beyond the $k = 0$ edge of the MSW band, this part of the pulse signal is rapidly attenuated and lost.

In addition to these linear effects, MSW excitations can exhibit strong nonlinear effects at relatively low microwave power levels. For example [16], in the low microwave frequency regime below 3.3 GHz for MSBVW signals and below about 4 GHz for MSSW excitations with small wavenumbers such that $kS < 1$ is satisfied, where S denotes the thickness of the YIG film, the nonlinear response for YIG results in a sharp increase in the losses for input power levels on the order of 1 mW or so. The dynamic nonlinear response can also result in a power-dependent MSW frequency [17]. It is important to work at sufficiently low-powers to avoid such effects for a purely linear MSW device.

C. Measurement Details and Response Analysis

The experimental setup for the low-power delay line measurements is indicated by the block diagram in Fig. 4. This setup was used for the characterization of the passive MSW delay line in the MSSW, MSBVW, and hybrid MSBVW/MSSW configurations as well as the various active delay line configurations. The microwave source was a Hewlett Packard Model 83650A synthesized sweeper. This unit was used to generate continuous-wave (CW) microwave power at a carrier frequency from 4 to 6 GHz and at power levels up to 16 dBm. The microwave switch was custom-produced by Alpha Industries, Inc. The rise time was below 1 ns and the isolation was 25 dB. The pulse generator was a Hewlett Packard Model 8161A programmable pulse synthesizer. The switch-pulse generator combination was used to produce microwave pulses with durations of 5–100 ns, rise times below 1 ns, and a dynamic range of about 25 dB.

As indicated by the block items on the right side of Fig. 4, the system was used for two types of measurements. Measurements of the insertion loss I and the one-pass delay time T versus frequency for the various passive delay line configurations were made with CW microwave excitation by means of a Hewlett Packard Model 8510C network analyzer. Time domain measurements of input and delayed microwave pulse characteristics and measurements of the power response of the various components of the feedback system were made with a Hewlett Packard Model 70 820A microwave transition analyzer. All data were collected and analyzed through a PC.

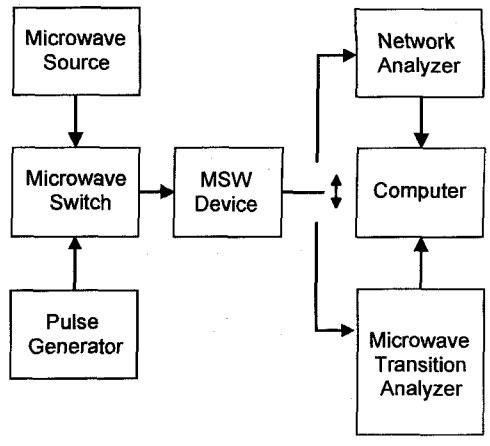

Fig. 4. Block diagram of the microwave measurement system.

The analysis of MSW wave packet propagation is often based on the nonlinear Schrödinger (NLS) equation [18]. For an MSW packet in a thin ferrite film, the NLS equation may be written as [19]

$$i\left[\frac{\partial u}{\partial t} + V_g\frac{\partial u}{\partial z} + \eta u\right] + \frac{1}{2}D\frac{\partial^2 u}{\partial z^2} - N|u|^2 u = 0. \quad (3)$$

Wave propagation is taken to be in the z-direction. The function $u(z, t)$ comprises a complex scalar envelope function that describes the MSW wave packet dynamic magnetization amplitude as a function of time t and propagation coordinate z. This function is typically normalized, so that $|u(z, t)|$ is on the order of $|\mathbf{m}|/M_s$, where $\mathbf{m}$ is the dynamic magnetization response for the MSW signal and M_s is the saturation magnetization of the YIG material. For YIG, $4\pi M_s$ is typically 1750 G. For the linear or small signal regime, $|\mathbf{m}|/M_s$ is typically well below 0.01. For nonlinear waves, this ratio may be well above 0.01. For the work presented below, $|\mathbf{m}|/M_s$ is well below this limit.

The square bracket term on the left-hand side of (3), taken alone, describes dispersionless propagation of a MSW packet envelope with group velocity V_g and temporal relaxation rate η. Typical values of $|V_g|$ and η are in the 10^6–10^7 cm/s and 10^6–10^7 rad/s range, respectively. Apart from numerical factors on the order of unity that depend on the specific geometry, η is related to the usual FMR half power linewidth ΔH by the relationship $\Delta H = 2\eta/|\gamma|$. The electron gyromagnetic ratio γ is specified by $|\gamma|/2\pi = 2.8$ MHz/Oe. The D term in (3) leads to a spreading out and drop in peak power for the MSW packet as it propagates. The D parameter is the dispersion coefficient, defined according to $D = 2\pi\partial^2 F(k)/\partial k^2|_o$. The dispersion coefficient is evaluated at the chosen operating point in frequency and wavenumber (f_o, k_o).

The N term brings in the effect of the nonlinear response on the MSW wave packet propagation to lowest order. The experiments discussed below have been limited to power levels well below those for which nonlinear effects are important. Equation (3) with N set to zero will be the basis for the analysis of the various MSW pulse propagation results to be presented in the sections that follow.

III. Passive and Active MSSW Delay Line

A. Passive Delay Line Properties

Consider first the CW signal frequency characteristics of the passive MSSW delay line. The MSSW line utilized a long, narrow YIG filmstrip, which was 2.16 mm wide, 16 mm long, and 15.7 μm thick. The transducer structure consisted of two shorted strip line transducers 50 μm in width and 2.5 mm in length placed apart by a distance $\Lambda = 1$ cm on separate single ground plane alumina substrates. These strip lines were used to excite and detect the MSSW signals in the film. The entire transducer structure and YIG film assembly was placed between the poles of an electromagnet in a uniform static magnetic field H_{ext}. For the CW and pulse MSSW measurements, the field was set at $H_{\text{ext}} = 950$ Oe. This field value was chosen to give MSSW propagation in a 4–5 GHz frequency passband and with minimal nonlinear effects for powers below 10 mW or so.

The measured frequency-dependences of the insertion loss, the one-pass delay time for the passive MSSW delay line, and the resulting insertion loss p.u. delay response parameter L, are shown in Fig. 5(a)–(c), respectively. The solid lines denote the results of the measurements. The solid dots show the results of theoretical modeling to be considered shortly. The data in Fig. 5(a) clearly show the MSSW passband between 4.5 and 5 GHz. This passband has a minimum insertion loss of about −8.8 dB at a frequency of 4565 MHz. This frequency will be taken as the operating frequency point f_o for the pulse experiments to be considered shortly. The insertion loss over the passband is smoothly varying and is not decorated by deep notches characteristic of YIG films with pinned surface spins. The films utilized for all the passive MSW devices considered in this and succeeding sections had unpinned surface spins.

Fig. 5(b) shows the wide variations that occur for the delay time over the SW passband. These changes are due to the shape of the dispersion curve of frequency versus wavenumber for surface waves. This dispersion results in a change in the MSW wave packet group velocity from a large value on the order of 1×10^6 to 5×10^6 cm/s near the lower edge of the passband to much smaller values at frequencies approaching 5 GHz. The decrease in V_g for frequencies approaching 5 GHz leads to the large delay times and the large insertion loss as well. The shape of the frequency profiles shown in Fig. 5(a) and (b) were independent of power up to 16 dBm or so. This provided good evidence for linear operation. Keep in mind that for the pulse measurements, a pulsewidth of 40 ns or so will correspond to a frequency spectral width on the order of 100 MHz. For frequencies within ±50 MHz of the 4565-MHz operating point, the delay time only varies from about 83 to 100 ns. For narrower pulses, the large spectral width can lead to problems related to dispersion and filtering. These points will be considered in more detail in the next section.

The solid dots in Fig. 5(a) and (b) show theoretical results. For these calculations, the well-known dispersion relation for the MSW surface mode frequency f_k versus in-plane wavenumber k for a insulating magnetic film of infinite lateral extent was used [14]. In this configuration, of course, the static

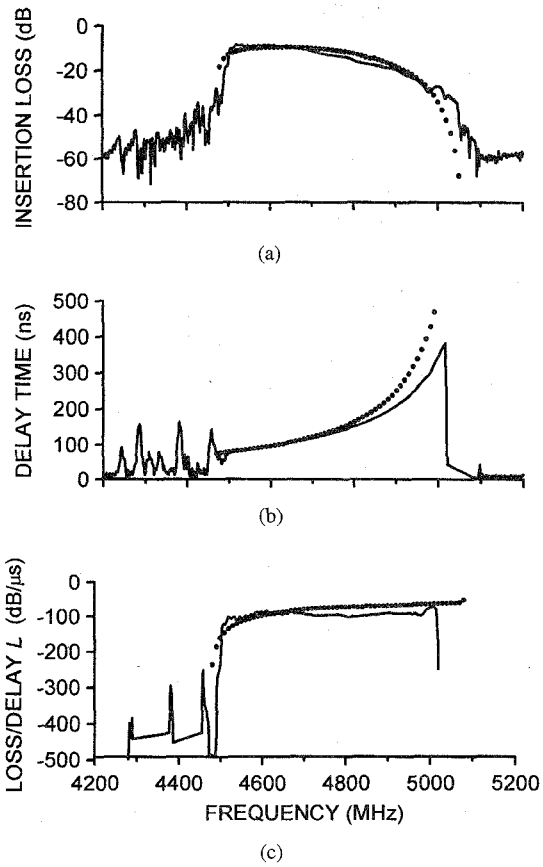

Fig. 5. Characteristic response curves for the passive MSSW delay line described in the text. (a)–(c) show the insertion loss, the delay time, and the loss p.u. delay time parameter L versus frequency, respectively. The solid lines show the data and the solid dots indicate the results of theoretical modeling as described in the text. The YIG film had a thickness of 15.7 μm and the in-plane static magnetic field was 950 Oe.

magnetic field is in-plane and perpendicular to the propagation direction. The MSSW frequency for an infinite film is given by

$$f_k = F(k) = \sqrt{f_H^2 + f_H f_M + \frac{f_M^2}{4}(1 - e^{-2kS})}. \quad (4)$$

In the above, f_H and f_M are frequency parameters defined by $f_H = (|\gamma|/2\pi)H$ and $f_M = (|\gamma|/2\pi) \cdot 4\pi M_s$, where H is the static internal magnetic field and S is the thickness of the film. After differentiation to obtain the group velocity $V_g(f_o)$, an analytical expression can be obtained for the MSSW one-pass delay time T for an operating point central frequency f_o and a propagation distance Λ

$$T(f_o) = \frac{\Lambda}{V_g} = \frac{1}{2\pi}\frac{\Lambda}{S}\frac{f_o}{(f_H + f_M/2)^2 - f_o^2}. \quad (5)$$

Numerical values $|\gamma|/2\pi = 2.8$ MHz/Oe and $4\pi M_s = 1750$ G, typical for YIG and as cited above were used for the numerical evaluations of the delay time. The static internal field H for the calculations was set at 947 Oe to adjust the theoretical value for the low-frequency edge of the MSSW band, given by $f_B = [f_H(f_H + f_M)]^{1/2}$, to the observed band edge of 4475 MHz from the data in Fig. 5. The small difference between experimental value of the static external field of 950 Oe and this H-value is due to demagnetizing

effects. For the film thickness and film width used here, the demagnetizing field can be on the order of 10 Oe.

The theoretical insertion loss curve in Fig. 5(a) was calculated by the method described in [20]. The various dimensions of the delay line structure, the magnetic parameters cited above, the nonuniform distribution of microwave currents across and along the strip line transducers, accurate matching conditions, and the MSSW magnetic propagation losses are all taken into account through the modeling procedure of [20]. The magnetic loss was based on a measured ferromagnetic resonance half-power linewidth ΔH of 0.8 Oe at 9.3 GHz.

For the active MSSW delay line measurements, this delay line configuration will be used with an operating point frequency f_o of 4565 MHz. As noted above, this point corresponds to minimum insertion loss. This frequency is about 100 MHz above the low-frequency band edge at f_B. This separation was deemed adequate to support the full frequency content of the 10–50 ns pulses used for the active MSSW delay line experiments. At this operating point frequency, the measured and calculated insertion losses were −9.0 and −9.5 dB, respectively. The measured and calculated delay times were 89.9 and 90.0 ns, respectively. The small differences between these measured and calculated values near the high frequency edge of the MSSW band may be related to the oversimplistic dispersion relation of (4) for narrow YIG filmstrips and the related nonuniformity in the static-internal magnetic field near the film edges. More accurate calculations of the MSSW dispersion in YIG film that take into account such effects could be carried out by the methods described in [21].

Fig. 5(c) shows measured and calculated results on the passive MSSW delay line loss p.u. delay time parameter L, in dB/μs, versus frequency. These results were obtained by dividing the corresponding insertion loss and delay time results in the upper parts of the figure. Note that the experimental loss p.u. delay time is practically independent of frequency over most of the entire MSSW passband. The average L is close to −100 dB/μs. The increase of insertion loss and the increase of delay time with increase in the frequency almost completely compensate each other. The calculated dependence for L [dB/μs] shows the same result. The theoretical limiting best case value of L, as estimated from the FMR linewidth [7], is on the order of −50 dB. The extra loss p.u. delay in Fig. 5(c) is likely due to paramagnetic losses in the GGG substrate [22] and additional MSSW scattering due to film surface roughness [23]. The main point of reference to be derived from Fig. 5 and the above discussion is that a benchmark loss p.u. delay parameter L for typical passive MSSW delay lines is in the −50 to −100 dB/μs range. It will be important to compare corresponding values of L for active delay line configurations with this benchmark.

B. Active MSSW Delay Line

The passive MSSW delay line described above was then used in the feedback arrangement shown in Fig. 1 to produce an active delay line. The feedback amplifier was a GaAs monolithic amplifier with the gain coefficient G of 31 dB and maximum output power of 0.5 W within the 2.5–6-GHz amplifier passband. The variable microwave attenuator in the feedback loop provided control of the overall feedback from changes in the attenuation A from 0 to −120 dB. The coupling coefficients of the directional couplers labeled B_{in} and B_{out} in Fig. 1 were both −3 dB. The passive MSSW delay line was set up with the same parameters as given in the previous section.

This active delay line was used to generate sequences of output pulses as described above for a range of input pulsewidths from 10 to 50 ns and for an input peak power of 10 mW. The input pulse repetition period was 1 ms. The input pulse carrier frequency was set at the operating point already indicated, $f_o = 4565$ MHz. This frequency corresponds to the middle of the MSSW passband region with a flat frequency response and a minimum insertion loss.

Fig. 6 shows example output pulse sequences for different values of the feedback attenuator setting A. Fig. 6(a)–(c) is for $A = -21$ dB, $A = -17$ dB, and $A = -13$ dB, respectively. The input pulsewidth for these results was 40 ns. The time axis is referenced to the leading edge of the first-pass output pulse. The second pulse in each sequence has a delay time T that corresponds to the second pass through the MSSW delay line; the third pulse has a delay time of $2T$, and so forth. The limiting value of the attenuation A for any pulse output was about −50 dB. As the graphs in Fig. 6 show, one obtains a gradual decrease in the pulse-to-pulse decay as the attenuation A is decreased. Fig. 6(c) for $A = -13$ dB represents the lowest practical value of attenuation for which a sequence of pulses could be obtained without the circuit going into oscillation. In Fig. 6(c), one can distinguish about nine well-separated undistorted pulses with a cumulative useful delay time of about 0.6 μs. This useful delay time, over which the delayed pulses maintain their integrity, will be defined as $(nT)_U$. For cumulative delay times longer than $(nT)_U$, the pulse train shows significant degradation. The individual pulses are still resolvable for times above 1 μs or so, but it is clear that severe distortion and overlap are beginning to affect the pulse train integrity. As discussed below, this degradation is due to the strong dispersion of MSSW delay line.

The effect of dispersion on the pulse broadening and the decrease in the peak power for successive pulses in the feedback sequence will be an important consideration. These effects may be estimated by considering the propagation of a low-power Gaussian pulse with the loss parameter η and the nonlinear parameter N in (3) set to zero. Let the initial pulse be described by a scalar function $u_o(t)$ of the form

$$u_o(t) = \mu_o e^{-(t^2/2\Delta_o^2)} \tag{6}$$

where μ_o is the initial pulse amplitude, Δ_o is a Gaussian width parameter and the peak of the pulse is taken to be at time $t = 0$ for a position $z = 0$. Note that the $1/e$ temporal width of the power profile $[u_o(t)]^2$ is equal to $2\Delta_o$. Standard Fourier techniques may be used in conjunction with (3) in the limit of zero loss and no nonlinear response to obtain a complex scalar time-dependent amplitude function $u_\tau(t)$ for the pulse at some position Z. The subscript τ denotes the propagation time for the pulse maximum from the point of launch at $z = 0$ to position Z. This time is given simply by $\tau = Z/V_g$.

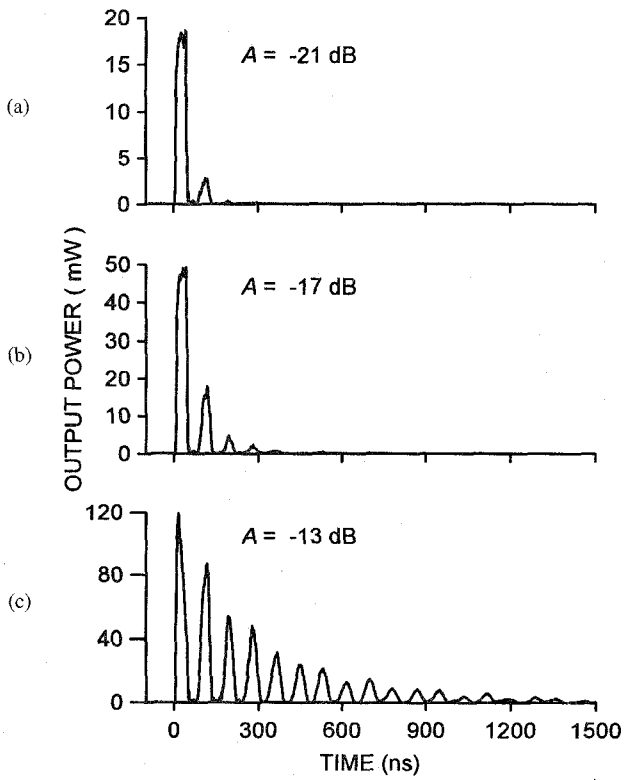

Fig. 6. Traces of output power versus time which show representative output pulse sequences for the active MSSW delay line described in the text. The static external field was 950 Oe, the input pulsewidth was 40 ns, the carrier frequency was 4645 MHz, and the input pulse peak power was 10 mW. (a)–(c) are for different values of the feedback attenuation A, as indicated. Time is referenced to the leading edge of the input pulse.

It will prove convenient to define a so-called dispersion time T_d according to $T_d = \pm\Delta_o^2 V_g^2/D$. The $\pm$ sign corresponds to positive or negative D, respectively, so that T_d is always positive. The physical significance of T_d will be apparent shortly. The complex $u_\tau(t)$ function for the propagated pulse at $z = Z$ is obtained as

$$u_\tau(t) = \frac{\mu_o}{\sqrt{1 \mp i\tau/T_d}} e^{-[(t-\tau)^2/2\Delta_o^2(1\mp i\tau/T_d)]}. \quad (7)$$

It follows from (7) that a pure Gaussian pulse subject only to dispersion will maintain its shape during propagation, but will have a width that increases and a peak power that decreases. The temporal width parameter Δ_τ and the peak amplitude μ_τ for the pulse that passes position $z = Z$ at time τ will vary according to

$$\frac{\Delta_\tau}{\Delta_o} = \sqrt{1 + \left(\frac{\tau}{T_d}\right)^2} \quad (8)$$

and

$$\frac{\mu_\tau}{\mu_o} = 1 \Big/ \left[1 + \left(\frac{\tau}{T_d}\right)^2\right]^{1/4}. \quad (9)$$

Equation (8) provides a basis upon which to estimate the time for an MSW pulse train to degrade to a point where the individual pulses are no longer discernable. From Fig. 6(c), this time appears to be somewhat greater than 1 μs.

The dispersion time T_d may be evaluated for the operating point and pulse conditions applicable to the data. First, evaluate the group velocity V_g and the dispersion coefficient D at the operating-point carrier frequency f_o and wavenumber k_o for the given field value H and other parameters as specified above. This may be done from the dispersion equation of (4) or the time delay result of (5). These parameters may be obtained directly from the delay time data of Fig. 5 as well. The group velocity is simply the transducer separation Λ divided by the delay time T at the operating point. The dispersion coefficient D may be obtained as $D = (1/2\pi)(\Lambda^2/T^3)[\partial T(f)/\partial f]|_{f_o}$. For the operating point of 4565 MHz, the data in Fig. 5 yield a delay time of 90 ns and a $\partial T/\partial f$ response of 0.17 ns/MHz. In combination with the Λ-value of 1 cm, $V_g = 11.1 \times 10^6$ cm/s and $D = -3.71 \times 10^4$ cm^2/rad·s are obtained. If 40 ns is taken as the width T_o for the input pulse used for the data in Fig. 5 to correspond to the $1/e$ width for the initial normalized power profile $[u_o(t)]^2$, $\Delta_o = T_o/2 = 20$ ns and a corresponding dispersion time T_d of 1330 ns result. For a delay time between pulses of 90 ns, the time for pulses to overlap would correspond to an increase in pulsewidth from 40 ns to about 90 ns, or a factor of 2.25. From (8), this corresponds to a propagation time of about 5.4 μs. This estimated time for overlap is about a factor of three to four times greater than the time scale in Fig. 6(c) and is about the right time inferred from those data for complete overlap.

The input microwave pulses in the experiments were square pulses rather than Gaussian. For a Gaussian pulse given in the form of (6) with a power profile $[u_o(t)]^2$ $1/e$ width of T_o as used above, the $1/e$ width of the Fourier frequency distribution is approximately equal to $0.9/T_o$. For a square pulse of width T_o and carrier frequency f_o, the Fourier frequency distribution $W(f)$ is of the form

$$W(f) = \frac{4\mu_o}{\sqrt{2\pi}} \frac{\sin[\pi(f - f_o)T_o]}{\pi(f - f_o)T_o}. \quad (10)$$

The width of this square pulse frequency distribution at the first zero and second zero crossing points is $2/T_o$ and $4/T_o$, respectively. The factor of 2–4 wider frequency distributions for the square pulse would indicate a dispersion decay for square pulses that is several times more rapid than obtained from simple Gaussian estimations [24]. Decay due to damping has also been neglected in the analysis. The simple estimation given here, therefore, may be considered to be in reasonable agreement with the observed degradation after 1 μs or so.

Measurements of pulse decay similar to the results shown in Fig. 6 were used to determine a loss p.u. delay time parameter L as a function of the feedback loop gain. Fig. 7 shows the variation of this loss p.u. delay time parameter L in dB/μs as a function of the feedback loop attenuator setting A. This loss per delay parameter L will be the key measure of the active delay line performance. The L-values shown in Fig. 7 were obtained from amplitude decay rate measurements over a limited delay time range of 0–0.5 μs to avoid false decay values for times where pulse overlap occurs. The operating parameters for the results in Fig. 7 were the same as for Fig. 6. The horizontal dashed line at -100 dB/μs indicates the nominal -100 dB/μs L-value shown in Fig. 5 for the

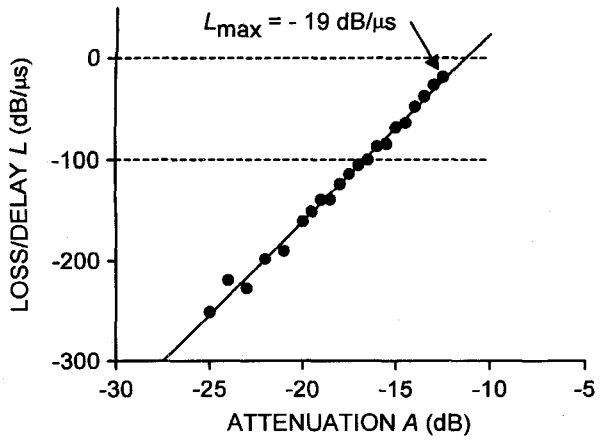

Fig. 7. Loss p.u. delay time parameter L as a function of the feedback loop attenuation A, based on pulse decay data of the sort shown in Fig. 6. The L-values are based on the drop in pulse amplitude over a delay time range from 0 to 0.5 μs. The frequency, field, input pulsewidth, and other operating parameters were the same as for Fig. 6. The input pulsewidth was 40 ns. The dashed lines provide reference points as discussed in the text. The indicated $L_{\max}$ value represents the largest value of L at the smallest attenuation that could be achieved experimentally before oscillation occurred.

passive MSSW device. The solid line represents a linear best fit to the data. The horizontal dashed line at 0 dB/μs indicates the maximum theoretical possible, L-value of 0 dB/μs, which would occur just before oscillation occurs.

The maximum value of L that could be achieved experimentally was somewhat smaller than the 0 dB/μs theoretical limit, as indicated by the $L_{\max} = -19$ dB/μs value in the figure. This $L_{\max}$ value was obtained at $A = -12.5$ dB. The change in L with A is well described by the straight line fit. The slope of the linear best fit response is 18.6 μs^{-1}. Extension of the linear best fit line to the theoretical limiting case zero loss line gives an A value of -11.4 dB. Therefore, the experimental limit on A before oscillation took place is about 1.1 dB below the theoretical limit.

It is also seen that the feedback at $A \approx -16.7$ dB produces a loss p.u. time performance factor of -100 dB/μs, the L-value for the passive device. This value is 5.3 dB below the -11.4 dB value of A at the theoretical zero decay limit. This gives a total loop loss of -5.3 dB.

The results in Figs. 6 and 7 are for an input pulsewidth of 40 ns. A few brief comments are in order concerning the effect of pulsewidth on the response characteristics of the active delay line. Measurements similar to those of Fig. 7 show that as the input pulsewidth is increased above 30 ns or so, the L-parameter levels off at values close to those shown in Fig. 7. For input pulsewidths below 30 ns, one observes a sharp decrease in L. There are two main origins for this drop in the L-parameter with decreasing input pulsewidth. The first is dispersion. The second involves band-pass filtering effects. As discussed above, the dispersion time scales with the square of the input pulsewidth. At a nominal input pulsewidth of 40 ns, the dispersion time as defined above is approximately 1300 ns. If the input pulsewidth is reduced by a factor of 4–10 ns, the dispersion time drops to about 80 ns. This results in rapid dispersion-broadening and a more rapid decrease in the peak power of the short microwave pulses as well.

Filtering effects occur because of the increased spectral width for short pulses in combination with the limited width of the useful part of MSSW frequency passband. From the above discussion on frequency distributions, a 40 ns pulse has a frequency spectrum that is about 100 MHz wide. For the situation in Fig. 5, with the MSSW frequency operating point at 4565 MHz, the passband low-frequency cutoff at 4475 MHz, and an increase in insertion loss for frequencies above 4700 MHz or so, a 40-ns wide pulse can pass through the delay line without additional distortion. On the other hand, a rectangular pulse of 10-ns duration has a frequency width of about 400 MHz. Because of the higher insertion loss in the passband for frequencies above the flat top region of the frequency response shown in Fig. 5 as well as the close proximity low-frequency band edge cutoff, the high- and low-frequency components of this 10-ns pulse are attenuated. This results in additional broadening of the output pulse signal and a more rapid decay.

In closing this section, consider the effect of interference between dispersed overlapping pulses after a long delay time. This interference results in a frequency-dependent decay rate for the active device. Both measurements and simple interference calculations give a frequency spacing of about 10 MHz between interference maxima for the output pulse amplitude after long delay times. This interference is one possible source of the premature onset of oscillation before one is able to attain the theoretically possible $L = 0$ dB/μs condition for the active device at the A-value corresponding to $G = 0$. Recall from the results in Fig. 7, for example, that it was not possible to attain the theoretical limit at $L = 0$ dB/μs due to the onset of oscillation for A-values below -11.4 dB. Due to the periodic change in the overall loop gain with frequency discussed above, oscillation starts before one reaches the $L = 0$ dB/μs point.

It is important to note that the broadening and interference effects discussed above are cumulative. The distortions that result cannot be circumvented through the use of cascaded passive delay lines to make up an active delay line with a longer single-pass delay time and additional amplifiers to make up the overall gain [8].

IV. Active Nondispersive Delay Line

The active MSSW delay line device presented in the previous section demonstrates the principle, the possibilities, and the limitations of the active feedback concept for long delay times at respectable decay rates. The limitations on device performance derive primarily from dispersion. In order to eliminate the detrimental effects of dispersion, a second active delay line has been developed that utilizes a nondispersive passive MSW delay line following the principle suggested by Sethares *et al.* [25]. The passive delay line consisted of two separate delay lines connected in series. The first individual delay line was an MSSW line of the sort used in the previous section. As shown in Fig. 5, the MSSW dispersion is such that the delay time increases with frequency. This dispersion was the source of the problems at long delay times. The second individual delay line was an MSBVW line. For magnetostatic backward volume waves, the dispersion is

such that the delay time decreases with increasing frequency. Through a suitable combination of these two different types of delay lines, with appropriate static magnetic fields, YIG film thicknesses, and transducer separations, it is possible to match the frequency passbands and achieve a delay time that is essentially independent of frequency.

The MSSW delay line for this hybrid device was the same as described above, but with a static magnetic field of 915 Oe. The MSBVW delay line was similar to the MSSW line, except that the static magnetic field was parallel to the direction of propagation. This MSBVW configuration is shown in Fig. 2 and discussed in Section II. This device made use of a second 15.7 μm thick YIG film. This filmstrip was 2 mm $\times$ 25 mm in size and had the same material properties as described above. Two shorted strip line transducers 50 μm wide and 2.5 mm long were placed 0.6 cm apart on the alumina substrate. This structure, with the YIG film on top, was placed between the poles of a permanent $SmCo_5$ magnet such that the static magnetic field was parallel to the long direction of the film strip and the propagation direction of the MSW signal. Near the central part of the film, the static magnetic field was 992 Oe.

The passive device characterization procedure was the same as for the MSSW delay line. The insertion loss and the one-pass delay time for the passive MSBVW line decrease with frequency, as expected for the inverted dispersion character. These characteristics are standard and will not be presented in detail. The usable MSBVW passband was between about 4400 and 4600 MHz. The minimum insertion loss was about -22 dB at about 4530 MHz. As in the previous section, this response is characteristic of YIG films with unpinned surface spins. The delay time decrease over the passband was from 120 to 80 ns. As in the MSSW case, the frequency profiles of loss and delay time were independent of power up to 16 dBm or so. These loss and delay profiles could be tuned by changing the position of the delay line structure in the inhomogeneous field of the permanent magnet used for the static magnetic field bias. This adjustment was used to tune the performance of the MSBVW delay line to achieve the desired nondispersive response for the overall two-stage delay line. The combined results on insertion loss and delay time gave a loss p.u. delay time parameter which peaked at about 4530 MHz and had a value close to -240 dB/μs.

The insertion loss, delay time, and loss p.u. delay time profiles for the MSSW delay line at $H = 915$ Oe were similar to the results shown in Fig. 5. There was a small downshift in frequency, of course, due to the decrease in the static field. This shift was needed in order to match up the profiles for the MSSW and MSBVW delay lines to produce the nondispersive delay line to be considered below.

The measured frequency dependences of the insertion loss, the one-pass delay time, and the resulting insertion loss p.u. delay response parameter L for the hybrid MSSW/MSBVW delay line are shown in Fig. 8(a)–(c), respectively. The format is the same as for Fig. 5. The solid lines denote the results of the measurements and the solid dots show the results of the theoretical modeling. The data in Fig. 8(a) show the combined passband from 4400 to 4600 MHz and the passband insertion loss of about -15 to -25 dB. Fig. 8(b) shows the delay time over the passband. Here, in contrast with both the MSSW case and the MSBVW case, the delay time is essentially constant over the passband. If one selects an operating point frequency at $f_o = 4530$ MHz, which corresponds to the minimum insertion loss frequency for the hybrid structure, the delay time is equal to 186 $\pm$ 3 ns for a 200-MHz band around this point. The loss p.u. delay time parameter L as a function of frequency for the hybrid device is shown in Fig. 8(c). The hybrid device has a minimum L-value of about -185 dB/μs, which is relatively constant over the device passband. While the L-parameter was also relatively frequency-independent for the MSSW delay line of Section III, this property was due to a compensation between the growth in insertion loss and growth in the time delay with frequency. For the hybrid delay line, all three parameters are more-or-less frequency-independent and, in particular, the time delay is frequency-independent.

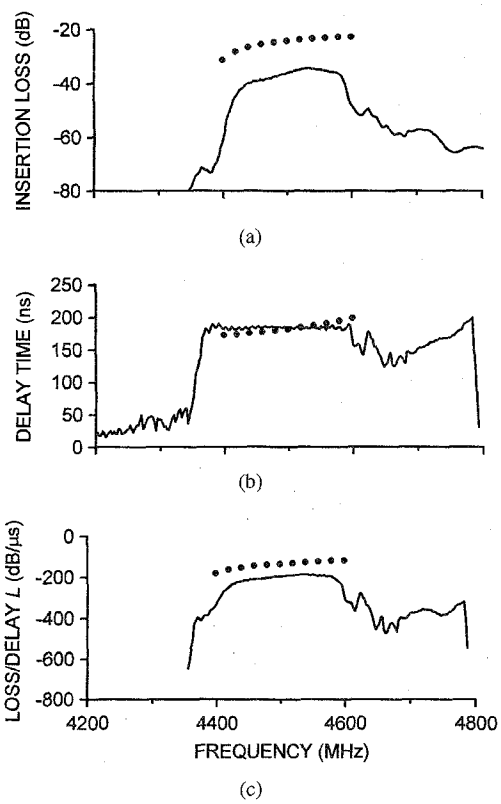

Fig. 8. Characteristic response curves for the hybrid MSSW/MSBVW delay line described in the text. (a)–(c) show the insertion loss, the delay time, and the loss p.u. delay time parameter L versus frequency, respectively. The solid lines show the data and the solid dots indicate the results of theoretical modeling as described in the text. Parameters for the hybrid structure are given in the text.

As in the MSSW delay line case, the solid dots show the results of simple device modeling calculations. Here, as in the MSBVW case, the discrepancy between the measured and calculated characteristics of the combined nondispersive MSSW/MSBVW line is due to the nonuniformity in the external magnetic field for the MSBVW line which was not taken into account in the calculations. Note that the delay time prediction is quite close to the measurement. The shapes of the theoretical response for the insertion loss and loss p.u. delay time graphs follow the shape of the data but with a lower loss.

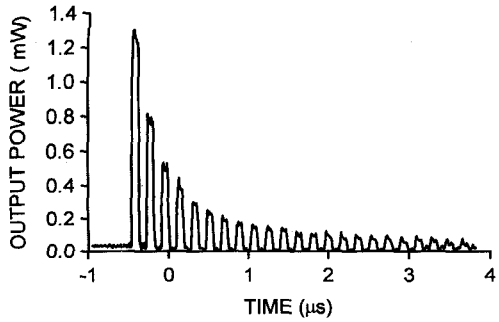

Fig. 9. Traces of output power versus time which show a representative output pulse sequence for the active hybrid MSBVW/MSSW delay line described in the text. The input pulsewidth was 100 ns, the carrier frequency was 4525 MHz, the input pulse peak power was 10 mW, and the feedback attenuation A was -2.5 dB.

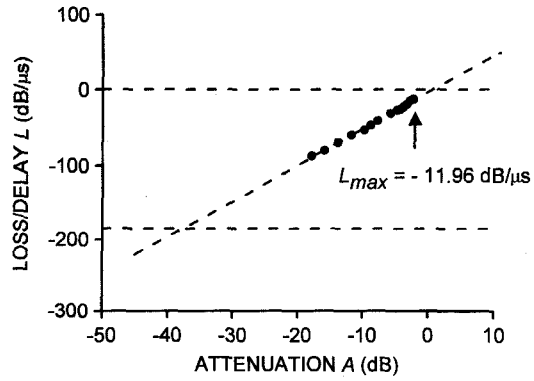

Fig. 10. Loss p.u. time parameter L as a function of the feedback loop attenuation A for the hybrid MSBVW/MSSW active delay line described in the text, based on pulse decay data of the sort shown in Fig. 9. The L-values are based on the drop in pulse amplitude over a delay time range from 0 to 0.5 μs. The operating parameters were the same as for Fig. 9. The input pulsewidth was 100 ns and the operating point frequency was 4525 MHz. The dashed lines provide reference points as discussed in the text. The indicated $L_{\max}$ value represents the largest value of L at the smallest attenuation that could be achieved experimentally before oscillation occurred.

The hybrid MSBVW/MSSW device was then used as the passive delay line element for a second active delay line configuration. The overall setup was similar to the setup shown in Fig. 1, but with several modifications. The delay line element now consisted of two passive delay lines in series, the MSSW delay line followed by the MSBVW line. The B_{in} and B_{out} coupling coefficients were -16 and -20 dB, respectively. In addition to the feedback amplifier shown in Fig. 1, a second amplifier was placed between the MSSW and MSBVW line elements to compensate for the additional insertion loss. This amplifier was a low power GaAs monolithic microwave amplifier with $G = 23$ dB and a maximum output power of 20 mW over the 4.2–6-GHz passband. For the active delay line measurements, 100-ns wide microwave pulses with an input peak power of 10 mW and a time separation of 1 ms were used. The operating-point carrier frequency was set at $f_o = 4525$ MHz, the frequency for the minimum insertion loss for the hybrid MSBVW/MSSW passive delay line.

Fig. 9 shows a sequence of delayed pulses from the active nondispersive MSW line for an input pulsewidth of 100 ns and an attenuator setting $A = -2.5$ dB. The format is the same as for Fig. 6, with output power on the vertical axis and time, relative to the leading edge of the input pulse, on the horizontal axis. The input power was 10 mW. Here, about 20 well-separated delayed pulses with cumulative useful delay time of about 3 μs can be seen. The significant enhancement in pulse integrity in Fig. 9 in comparison with the data in Fig. 6(c) is clear. Due to the lack of dispersion spreading, the pulses conserve their shape almost to the limit of the data shown. It is clear from these data that the dispersion time is much greater than the 4-μs time scale of the horizontal axis. The main source of pulse distortion for delay times greater than 3 μs is probably the narrow passband and filtering effects. The narrow passband shown in Fig. 8(a) results in a cutoff for sidelobe harmonics in the microwave pulse spectrum and a distortion of the pulse edges. The loss p.u. delay time parameter L for the pulse data in Fig. 9 is about -12 dB/μs. Recall that the attenuator setting for these pulse measurements was at $A = -2.5$ dB. This value of A was close to the smallest attenuation for which pulses could be obtained without circuit oscillation.

Fig. 10 shows experimental results on the variation of the L parameter with the attenuator setting A. The format is the same as for Fig. 7 and the procedure for the L-determinations was also the same. Amplitude decay rate measurements over a limited cumulative delay time range of 0–0.5 μs were used. The parameters were the same as for Fig. 9. The horizontal dashed line at -185 dB/μs indicates the nominal L-value shown in Fig. 8 for the passive hybrid delay line. The solid line shows a linear best fit to the data. The horizontal dashed line at 0 dB/μs shows the maximum theoretical possible L-value of 0 dB/μs which should occur just before the onset of oscillation.

As with the MSSW device, the maximum value of L that could be achieved experimentally was somewhat smaller than the 0 dB/μs theoretical limit, as indicated by the $L_{\max} = -11.96$ dB/μs value in the figure. This $L_{\max}$ value was obtained at $A = -2.4$ dB. The change in L with A is well described by the straight line fit. For this hybrid device, the slope of the linear best fit response is 4.85 μs^{-1}. Recall that the slope of the L versus A response for the MSSW active device was 18.6 μs^{-1}. The less rapid response for the hybrid device allowed for more precise tuning of A to obtain the maximum L. Extension of the linear best fit line to the theoretical limiting case 0 dB/μs loss line gives a theoretical limiting A value of +0.2 dB for the active hybrid device. The experimental limit on A of -2.4 dB before oscillation took place was about 2.6 dB below the theoretical limit. For the MSSW device, this difference was 1.1 dB. As before, this difference can be attributed to interference effects.

The intersection of the linear best fit line to the -185-dB/μs reference line indicates the A-value at which the active device produces a loss p.u. delay time performance factor that is just equal to the L-value for the passive hybrid device. For the hybrid device, this equivalence occurs at $A \approx -37.7$ dB. This value may be compared to the +0.2-dB value of A at the theoretical zero decay limit to set the total loss in the loop at -37.9 dB.

The above results demonstrate the improvements to the active delay line which can be obtained through the utilization of

a nondispersive passive delay line. The remaining limitations derive mainly from the lack of a flat frequency response for the hybrid passive delay line. The use of broadband, flat-response, nondispersive delay lines will allow an even better performance factor and the achievement of large delay times and low decay rate active devices.

V. Conclusion

The results presented above demonstrate the possibility to design an active MSW delay line which may be used to provide long delay times with a reduced decay rate for short microwave pulses. The active line consists of a passive MSW delay line and a microwave amplifier connected in the feedback loop. Microwave pulses are delayed in the passive MSW line while the amplifier compensates for the insertion loss. Two active delay line configurations have been considered, one based on a passive MSSW delay line and one based on a hybrid MSBVW/MSSW nondispersive passive delay line. The best-case result was for the nondispersive line, with a loss p.u. delay time parameter of -12 dB/μs and a maximum useful delay time of 3 μs or so, compared with typical L-values of -50 to -100 dB/μs and useful delay times of about 0.2 μs for passive MSW delay lines. These results were obtained for microwave pulses 10–100 ns in width for a carrier frequency in the 4–5-GHz range.

In order to further decrease the loss p.u. delay time and increase the useful delay time of the active MSW line, it will be necessary to: 1) eliminate broadening of MSW pulses during the multiple pass circulation in the passive delay line and 2) adjust the total loss coefficient of the feedback loop as close to unity as possible, but below the threshold for self-oscillation. The dispersion spreading of delayed pulses may be considerably decreased through the use of a nondispersive passive MSW delay line or the propagation of MSW solitons in the passive MSW line. In order to decrease the total loss in the feedback loop, one should use a broadband passive MSW line with flattop response and utilize feedback amplifiers which provide linear operation over the range of powers needed for the feedback signals. The broadband, flattop response is especially important for short microwave pulses or pulses with a significant frequency modulation, both of which result in signals with a wide frequency power spectrum.

Acknowledgment

The authors gratefully acknowledge Prof. A. N. Slavin, Prof. B. A. Kalinikos, and H. E. Ensle for helpful discussions.

References

[1] *Proc. 1981 RADC Microwave Magnetics Technol. Workshop*, June 10–11, 1981, J. C. Sethares, Ed., Rome Air Development Center, Griffiss AFB, NY 13441, In-House Rep. RADC-TR-83-15, Jan. 1983; also Special Issue on Magnetostatic Waves and Signal Processing, *Circuit Syst. Signal Process.*, J. P. Parekh, Ed., vol. 4, nos. 1–2, 1985.

[2] J. D. Adam, "Analog signal processing with microwave magnetics," *Proc. IEEE*, vol. 76, pp. 159–171, 1988.

[3] K. W. Chang, J. M. Owens, and R. L. Carter, "Linearly dispersive time-delay control of magnetostatic surface waves by variable ground-plane spacing," *Electron. Lett.*, vol. 19, pp. 4886–4887, 1983.

[4] L. R. Adkins and H. L. Glass, "Propagation of magnetostatic surface waves in multiple magnetic layer structures," *Electron. Lett.*, vol. 16, pp. 590–592, 1980.

[5] L. R. Adkins, R. L. Carter, K. W. Chang, H. L. Glass, J. M. Owens, and F. S. Stearns, "Electronically variable time delays using cascaded magnetostatic delay lines," *J. Appl. Phys.*, vol. 55, pp. 2518–2520, 1984.

[6] A. K. Ganguly and D. C. Webb, "Microstrip excitation of magnetostatic surface waves; Theory and experiment," *IEEE Trans. Microwave Theory Tech.*, vol. 23, pp. 998–1006, 1975.

[7] D. D. Stancil, "Phenomenological propagation loss theory for magnetostatic waves in thin ferrite films," *J. Appl. Phys.*, vol. 59, pp. 218–224, 1986.

[8] V. Priye and M. Tsutsumi, "Observation of short pulse in cascaded magnetostatic soliton waveguide," *Electron. Lett.*, vol. 31, pp. 464–465, 1995.

[9] L. F. Mollenauer and K. Smith, "Demonstration of soliton transmission over more than 4000 km in fiber with loss periodically compensated by Raman gain," *Opt. Lett.*, vol. 13, pp. 675–677, 1988.

[10] L. F. Mollenauer, M. J. Neubelt, S. G. Evangelides, J. P. Gordon, J. R. Simpson, and L. J. Cohen, "Experimental study of soliton transmission over more than 10,000 km in dispersion shifted fiber," *Opt. Lett.*, vol. 15, pp. 1203–1204, 1990.

[11] H. A. Haus, "Optical fiber solitons, their properties and uses," in *Proc. IEEE*, vol. 81, pp. 970–983, 1993.

[12] J. P. Castera, "Tunable magnetostatic-surface-wave oscillator," *IEEE Trans. Magn.*, vol. 14, pp. 826–828, 1978.

[13] W. S. Ishak, "Magnetostatic wave technology: A review," *Proc. IEEE*, vol. 76, pp. 171–179, 1988.

[14] R. W. Damon and J. H. Eshbach, "Magnetostatic modes of a ferromagnetic slab," *J. Phys. Chem. Solids*, vol. 19, pp. 308–320, 1961.

[15] R. W. Damon and H. van de Vaart, "Propagation of magnetostatic spin waves at microwave frequencies in a normally magnetized disk," *J. Appl. Phys.*, vol. 36, pp. 3453–3459, 1965.

[16] W. Shiltz, "Spin-wave propagation in epitaxial YIG films," *Philips Res. Rep.*, vol. 28, pp. 50–61, 1973.

[17] M. A. Tsankov, M. Chen, and C. E. Patton, "Magnetostatic wave dynamic magnetization response in yttrium iron garnet films," *J. Appl. Phys.*, vol. 79, pp. 1595–1603, 1996.

[18] V. I. Karpman, *Nonlinear Waves in Dispersive Media*. New York: Pergamon, 1973.

[19] A. K. Zvezdin and A. F. Popkov, "Contribution to the nonlinear theory of magnetostatic spin waves," *Zh. Exper. Teor. Fiz.*, vol. 84, pp. 606–615, 1983; also *Sov. Phys. JETP*, vol. 57, pp. 350–355, 1983.

[20] G. A. Vugalter and V. N. Makhalin, "Reflection and excitation of surface magnetostatic waves by a metal strip," *Zh. Tekh. Fiz.*, vol. 55, pp. 497–505, 1985; also *Sov. Phys. Tech. Phys.*, vol. 30, pp. 296–300, 1985.

[21] A. Yu. Annenkov, I. V. Vasiliev, S. V. Gerus, and S. I. Kovalev, "Magnetostatic surface wave modes in a channel created by a nonuniform magnetic field," *Zh. Tekh. Fiz.*, vol. 65, pp. 71–82, 1995; also *Sov. Phys. Tech. Phys.*, vol. 40, pp. 330–336, 1995.

[22] M. Maryško, "Influence of GGG substrate on FMR and magnetostatic wave propagation," *J. Magn. Magn. Mater.*, vol. 101, pp. 159–161, 1991.

[23] S. A. Nikitov, "Relaxation phenomena of magnetic excitation in ferromagnetic media," in *Relaxation Phenomena in Condensed Matter*, W. Coffey, Ed. (Advances in Chemical Physics Series), 1994, vol. LXXXVII, pp. 545–594.

[24] G. P. Agrawal, *Nonlinear Fiber Optics*. Boston, MA: Academic, 1995.

[25] J. C. Sethares, J. M. Owens, and C. V. Smith, "M.S.W. nondispersive electronically tunable time delay elements," *Electron. Lett.*, vol. 16, p. 825, 1980.

Yuri K. Fetisov (SM'96) was born in Moscow, Russia, on June 19, 1955. He received the M.S. degree in physics and the Ph.D. degree in solid state physics from the Moscow Engineering Physics Institute in 1978 and 1981, respectively., and the Doctor of Sciences degree in solid state physics from the Institute of Radioengineering and Electronics of Russian Academy of Sciences in 1993.

Since 1981, he has been working as a Researcher, Assistant Professor, Associate Professor, and Full Professor in the Department of Physics, Moscow Institute of Radioengineering, Electronics, and Automation (MIREA). He is presently the leader of the microwave and optoelectronics laboratory. His current research interests include magnetostatic spin wave physics and optical-microwave interactions in thin ferrite films, microwave signal processing, and optoelectronic devices and systems. He has written more than 60 papers in the area of magnetostatic spin wave physics and microwave signal processing devices based on thin ferrite films. He has held visiting appointments at Colorado State University (1995, 1997) and at Chiba University, Japan (1995).

Pavel Kabos (SM'93) received the M.S. degree in solid state physics in 1970 from the Electrotechnical Faculty of the Slovak Technical University and the Ph.D. and Doctor of Science (Dr.Sc.) degrees in electrical engineering in 1979 and 1994, respectively, from the Slovak Technical University, where he studied dynamic magnetization processes in bulk ferrites and thin films.

He joined the Department of Theoretical and Applied Electrical Engineering faculties at the Electrotechnical Faculty of the Slovak Technical University as an Assistant Professor in 1970, where he worked on microwave relaxation and nonlinear processes in ferrites. In 1983, he was advanced to the rank of Associate Professor. He spent 1982–1984 at the Department of Physics of Colorado State University as a Post-Doctoral Fellow, and in 1991 returned to Colorado State University where he is presently a Research Professor. His research includes work on microwave and millimeter wave ferrite materials, magnetic metals and alloys, Brillouin light scattering in magnetic systems, spin-wave instability and nonlinear microwave processes, off-resonance microwave losses and effective linewidth, excitations in magnetic superlattices, chaos, and microwave solitons in thin magnetic films. He has authored or coauthored one book and more than 65 publications in the archival technical literature on research in basic and applied magnetics.

Carl E. Patton (SM'71–F'89) was born in San Antonio, TX, on September 14, 1941. He received the B.S. degree in physics in 1963 from the Massachusetts Institute of Technology, Cambridge, where he investigated crystal field spectra at the National Magnet Laboratory, and the Master's and Ph.D. degrees in electrical engineering in 1964 and 1967, respectively, from the California Institute of Technology, Pasadena, where he studied dynamic magnetization processes in thin films.

He joined the Raytheon Research Division, Waltham, MA, in 1967, where he worked on microwave relaxation and nonlinear processes in ferrites. He joined the Physics faculty at Colorado State University, Fort Collins, in 1971 as an Associate Professor. In 1976, he was advanced to the rank of Professor. At Colorado State University, his research includes work on microwave and millimeter wave ferrite materials, magnetic metals and alloys, magnetism in lunar matter, Brillouin light scattering in magnetic systems, spin-wave instability and nonlinear microwave processes, off-resonance microwave losses and effective linewidth, excitations in magnetic superlattices, chaos, and microwave solitons in thin magnetic films. He has held various visiting appointments worldwide: Institute of Solid State Physics, University of Tokyo and Tohoku University, Sendai (1969–1970, Japan Society for the Promotion of Science Fellowship); Institute of Physics, Czechoslovak Academy of Science, Prague (1973 and 1979, National Academy of Science Exchange Fellowship); Institut fur Angewandte Festkorperphysik, University of Freiburg, West Germany (1977–1978, Alexander von Humboldt Research Fellowship); Department of Physics, Simon Fraser University, Burnaby, BC, Canada (1984–1985); NIST, Boulder, CO (1991–1992). He has authored or coauthored more than 150 publications in the archival technical literature on research in basic and applied magnetics. He has consulted with Westinghouse, Northrop Aviation, Boeing Aerospace, the US Army Electronic Technology and Devices Laboratory, and Northrop Grumman Corporation.

Dr. Patton is a Fellow of the American Physical Society. He has served as Newsletter Editor for the IEEE Magnetics Society (1973–1976), as a member of numerous program committees for the IEEE sponsored Intermag Conference and the Conference on Magnetism and Magnetic Materials, as a Reviews Editor for the IEEE TRANSACTIONS ON MAGNETICS (1984–1986), as Editor-in-Chief of the TRANSACTIONS (1987–1991), and as a member of the Administrative Committee, the Technical Committee on High Frequency Magnetics, and the Technical Committee on Education of the IEEE Magnetics Society. He served as Program Co-Chairman for the 1987 Conference on Magnetism and Magnetic Materials (Chicago) and was the General Chairman for the 1990 Conference (San Diego). He was an IEEE Magnetics Society Distinguished Lecturer for 1993 and 1994, with 58 lectures in six countries. He is the 1998 Chairperson of the American Physical Society Topical Group on Magnetism and its Applications. He has been the recipient of development awards, research grants, and contracts from various government agencies and industrial organizations such as the National Science Foundation, NASA, NATO, the U.S. Army, the U.S. Air Force, the US Navy, Verbatim, Ampex, Rockwell International, TRW, Honeywell, Sandia National Laboratories, and CMI Technology, with total funding in excess of 4.8 million dollars.